Transportation Research Part C 86 (2018) 563–579

Contents lists available at ScienceDirect

Transportation Research Part C

journal homepage: www.elsevier.com/locate/trc

Overview Paper

# 3D virtual intersection sight distance analysis using lidar data

Jaehoon Jung*, Michael J. Olsen, David S. Hurwitz, Alireza G. Kashani, Kamilah Buker

*School of Civil and Construction Engineering, Oregon State University, 101 Kearney Hall, Corvallis, OR 97331, USA*

ARTICLE INFO

*Keywords:*
Stopping sight distance
Intersection sight distance
Intersection safety
Lidar
3D viewshed

ABSTRACT

Sight distance analyses require careful and detailed field measurements to facilitate proper engineering decision making regarding the removal of obstructions, establishment of regulatory and advisory speed limits, and the location of new access points, among numerous other purposes. However, conventional field measurements for these analyses present safety concerns because they require personnel to be in or adjacent to traffic lanes. They can also be time consuming, costly, and labor intensive. Furthermore, the predominantly two-dimensional (2D) methods involve simplifying assumptions such as a "standard" vehicle heights and lengths without considering the wide range of vehicles and drivers present on the road. Recently, many transportation agencies worldwide have begun to acquire mobile lidar data to map their roadway assets. These data provide a rich three-dimensional (3D) environment that enables one to virtually visit a site at any frequency and efficiently evaluate sight distances from the safety of the office. This study investigates advanced safety analysis methodologies for drivers' sight distance based on high resolution lidar data. The developed simulation method enables users to virtually evaluate available sight distances in a 3D context considering a variety of objects, vehicle types, and multi-modal forms of transportation (e.g., bicycle, pedestrian). The feasibility of this technique was analyzed with a case study at an intersection located in Corvallis, Oregon, USA. The experimental results demonstrated the ability of the proposed methodology to capture significantly more detail on visibility constraints when compared with conventional measurements as well as provide more flexibility in the analysis.

## 1. Introduction

Sight Distance (SD) is the length of road visible to a road user measured from any point along the traveled way. A key component in the safe design, operation, and maintenance of highways is the provision of adequate SD (AASHTO, 2011; Fambro et al., 1997). Two categories of SD are Stopping Sight Distance (SSD) and Intersection Sight Distance (ISD). SSD is defined as the sum of the distance traversed by the vehicle from the instant the driver detects an object obstructing the forward progressing of the vehicle on the current path necessitating the driver to stop to the instant the brakes are applied (brake reaction distance) and the distance needed to stop the vehicle once the brakes have been applied (braking distance). In addition to SSD, SD must also be considered at intersections (commonly termed ISD) to provide drivers of stopped vehicles an adequate view of the intersecting highway to allow them to cross or enter the intersecting highway (AASHTO, 2011).

SD analyses require careful and detailed field measurements to facilitate proper engineering decision making regarding the removal of obstructions, establishment of regulatory and advisory speed limits, and the location of new access points, among

* Corresponding author.
*E-mail address:* jaehoon.jung@oregonstate.edu (J. Jung).

https://doi.org/10.1016/j.trc.2017.12.004
Received 17 August 2017; Received in revised form 7 December 2017; Accepted 9 December 2017
Available online 22 December 2017
0968-090X/ 

numerous other examples. Transportation facilities should be designed such that a driver has sufficient visibility to avoid collision with an object obstructing the traveled way. SD measurements and calculations are based on driver characteristics, vehicle types, road grade, horizontal and vertical curves in road, road conditions (e.g., wet surface), and the type of maneuver that the driver will perform.

Limited visibility is a principal cause of crashes in transportation corridors. Investigation of these cases showed that specific preventive safety practices could reduce the number of these fatalities. One solution is to identify obstacles and hazardous road or construction work spaces, which will allow for the selection of proper strategies such as removing obstructions, implementing safety warning signs, and optimizing blind spaces by alternating the road or construction site features and equipment locations.

Conventional field measurements of SD present safety concerns because they require personnel to be in or adjacent to active traffic lanes (e.g., McKinley, 2014). These studies are generally time consuming, costly, and labor intensive. Further, the methods that are currently used are based on 2D theoretical equations (AASHTO, 2011), which require simplifying assumptions such as a "standard" vehicle (height and length) without considering the wide range of vehicles present on the road. Another limitation in conventional SD analyses is that only static objects and vehicles are considered. This method does not enable one to model the dynamic motion of both vehicles and objects that occurs in the real world. They do not also consider multi-modal forms of transportation such as bicycles.

Lidar is a recent technology that can rapidly generate survey quality, 3D data of a scene, which can be utilized to analyze visibility within a space (e.g., Batchelor, 2016). A key benefit to lidar technology is the ability to utilize the same data source to support multiple applications including asset management, safety analyses, construction, planning, and maintenance. Lidar data provide a 3D environment that enables one to frequently visit a site virtually and obtain measurements from the safety of the office efficiently.

Recently, many transportation agencies worldwide have begun to acquire Mobile Lidar data for their highways (Olsen, 2013), which has a great potential for supporting a wide range of applications, such as condition evaluation of traffic signs and road markings (Ai and Tsai, 2016; Soilán et al., 2017), assessment of highway alignment (Marinelli et al., 2017), and simulation of vehicle dynamics (Brown and Brennan, 2015). Recently, Oregon DOT (ODOT) has completed mobile lidar surveys of all state owned and maintained highways and updates high priority areas annually (Mallela et al., submitted for publication). Among other purposes, ODOT utilized this data to manually extract measurements to perform virtual passing SD analyses of passing lanes in rural highways where speed limit increases were introduced. The efficiency of this approach resulted in $250,000 (US) savings compared to conventional technique.

This research explores the feasibility, benefits, and challenges of a 3D safety analysis for sight distances based on lidar data. Specifically, the following objectives were accomplished:

- Developed a systematic framework to utilize 3D laser scanning data to evaluate sight distances,
- Compared the framework to conventional techniques for validation,
- Evaluated visibility changes during vehicle movements such as turning,
- Considered differences in visibility based on different vehicles and multi-modal forms of transportation, and
- Provided 3D viewsheds that can help agencies manage SD obstructions.

The remainder of this paper is organized as follows. Section 2 reviews the latest developments in SD analysis using GIS, lidar and other 2.5D technologies that cannot account for the objects with the same horizontal locations but different elevations. Section 3 outlines the procedure of the proposed methodology in detail. Section 4 presents the description of the study site and point-cloud data collected for an intersection. Section 5 provides the test results of the proposed methodology with several visibility constraints. Finally, Section 6 identifies the potential utility of the proposed methodology and upcoming work.

## 2. Related works

Initial efforts of using geospatial data for SD analysis were related to the design phase of roads (Hassan et al., 1996; Ismail and Sayed, 2007; Jha et al., 2011; Jha and Karri, 2009). These methods used design alignments and terrain topographic information to simulate the road geometry and conduct SD calculations. However, a major limitation arises since they only consider the road geometry and ignore the influence of other effective objects such as trees, buildings, signs, etc. Moreover, these methods simplify the road geometry (e.g. constant road grade and cross slope) with assumptions.

Recent developments in Geographic Information Systems (GIS) and Digital Elevation Modeling (DEM) provided efficient tools that can be used for SD analysis of existing roads. GIS enables one to conduct line of sight analysis that is in accordance with the available GIS terrain and surface model and combine the result of such analysis with other sources of information such as crash statistics and speed limits for further evaluations. Table 1 summarizes studies that have performed geospatial visibility analysis for roads and highways.

The ArcGIS Line of Sight (LOS) and viewshed analysis tools have been used in some studies in Table 1 to determine Available Sight Distance (ASD) on roads (Castro et al., 2014, 2017; Khattak and Shamayleh, 2005) and intersections (Khattak et al., 2003; Tsai et al., 2011). Two main methods were reported. In the first method, which is often used for intersection SD analysis, a viewshed for a driver is first determined based on assumptions such as vision range, angle, and obstacle locations. Then, the intersection area included in the viewshed polygon is determined and the length of ASD is extracted. In the second method, which is typically used for road SD analysis, path points with equal distances are generated on a road trajectory polyline. Then, the GIS LOS tool is used to determine the farthest seeable point for each of the path points to generate the viewshed.

**Table 1**
Summary of related studies performing geospatial visibility analyses (modified from Olsen et al., 2015).

| Reference | Contribution | GIS function | Model used | Lidar used |
|---|---|---|---|---|
| Khattak et al. (2003) | GIS LOS method to detect intersection SD obstructions | LOS | First and last return DTM | ALS |
| Khattak and Shamayleh (2005) | GIS viewshed method to detect a road SD obstructions | Viewshed | DSM | ALS |
| Tsai et al. (2011) | GIS POS method to detect intersection SD obstructions and quantify the severity | Viewshed | DSM | ALS |
| Castro et al. (2011) | GIS viewshed method to calculate ASD on a highway | Viewshed | DTM | N/A |
| Castro et al. (2014) | GIS POS loops to calculate ASD on a highway and detect diving locations | LOS loop | DTM | N/A |
| De Santos-Berbel et al. (2014)–Castro et al. (2017) | Compare the influence of DTM and DSM made from ALS and MLS data on method presented in Castro et al. (2014) | LOS loop | DTM, DSM | ALS, MLS |
| Olsen et al. (2015) | 3D voxel-based method to calculate ASD at intersections | Viewshed | Point cloud | TLS |

The quality of the digital model used to represent the terrain and road objects' geometry directly affect the quality of SD analysis. Two types of digital models used are Digital Elevation Models (DEMs, sometimes referred to as digital terrain models, DTMs) and Digital Surface Models (DSMs). DEMs represent the bare ground surface. However, DSMs are more beneficial for SD analysis because they include other on the ground objects such as trees, buildings, walls, and traffic signs that would generate obstructions.

Note that the DSMs in most studies reported in Table 1 do not fully represent the geometry of 3D objects, which can adversely influence the SD analyses by not accounting for visible space underneath some objects such as tree crowns, building overhangs, signs, power lines, and tunnels located above the road surfaces. DSMs can be represented as a Triangulated Irregular Network (TIN), which are generated through a Delaunay triangulation. For a given set of points (e.g., a lidar point cloud), Delaunay triangulation is an aggregate of connected but non-overlapping triangles such that the circumcircle of each triangle has no other point in its interior (Delaunay, 1934; Tsai, 1993). In this technique, only the horizontal projection of points is used to form non-overlapping triangles. Point elevations are only considered after the triangulation is generated. Unfortunately, this technique does not fully support a 3D representation of surfaces because it generates only non-overlapping surfaces when projected to 2D. Therefore, the resulting DSM cannot include surfaces with the same horizontal locations but different elevations. For this reason, sometimes the method is referred to as 2.5D instead of 3D (De Santos-Berbel et al., 2014).

In the authors' previous work (Olsen et al., 2015), an algorithm was developed to automatically determine available SD at intersections using lidar point cloud data. In this technique, the 3D space is divided into small, cubic volume pixels called voxels. These 3D voxel-based structure is used to represent objects captured within the lidar data. This methodology resolves the "2.5D vs 3D" issue mentioned in the previous paragraph. The driver's lines of sight are also generated and used to determine areas visible to the driver. Finally, the GIS binary raster map identifying locales as visible or not is generated.

## 3. Methodology

In this work, a novel method is proposed for effective 3D sight distance analysis using point-cloud data as schematized in Fig. 1. First, the proposed methodology separates the ground points using a histogram method. The mean elevation of the ground points is calculated and added to the user-defined driver's height above the ground level to determine the appropriate elevation for the analysis. Then, the algorithm organizes the entire point-cloud onto an x-y plane to generate a grid representation of the road and surrounding objects. A line-of-sight analysis is performed on the grids to efficiently detect the object points in a driver's field of view, which are then evaluated in 3D space to determine where the driver's visibility is blocked for generation of a driver viewshed map. Finally, the viewshed maps with several visibility constraints are generated and compared with the conventional field measurements through both qualitative and quantitative evaluation. The method was designed to be flexible such that one can vary driver's position, height, and viewing angles as well as the desired level of detail of the results. Each step will be discussed in more detail in this section.

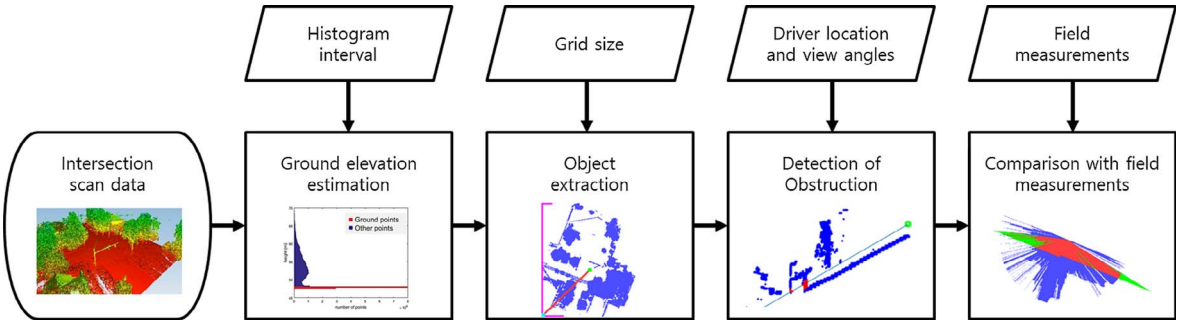


**Fig. 1.** Key steps in the Algorithm workflow.

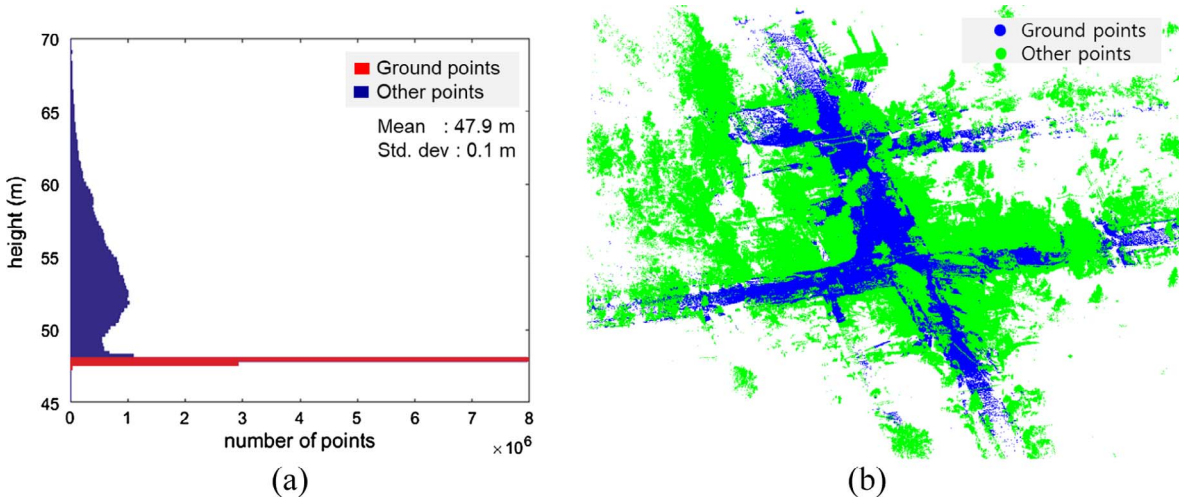


**Fig. 2.** Ground height estimation using a histogram method: (a) histogram representing number of points and (b) separated ground points from point cloud.

### 3.1. Ground elevation estimation

The initial step of the algorithm is to separate the ground points (potential obstructions) from a registered and cleaned point cloud. First, a histogram along the z-axis (elevation) is computed (Fig. 2a) with bin sizes of 0.4 m (Jung et al., 2017), ranging from the minimum to the maximum elevation. Next, the peak indicates the presence of the ground surface, which normally contains the largest number of points based on the scanning geometry and projected area occupied by the ground relative to other objects. Fig. 2b illustrates the separation of the ground and other points where points within the bin containing the peak and the bins lower than the peak are classified as ground. The mean elevation of the ground points is computed and added to the user-defined driver's height above the ground level to determine the appropriate elevation for the analysis. This method assumes that the ground surface is mostly constant in elevation (planar) and contains the largest number of points. This simplified method provides significant computational efficiency for most intersections; however, for cases in which the histogram method is not appropriate, e.g. intersections located in hilly terrain, a more rigorous ground filtering technique would be a viable solution (e.g., Che and Olsen, 2017) and will be taken into consideration in future work.

### 3.2. Object extraction

In this phase, the driver's lines of sight are generated and used to extract the objects visible to the driver. First, the whole point cloud is organized onto the x-y plane to create a grid representation: if a grid cell contains at least one projected point, it is represented as 1 (occupied grid); otherwise, as 0 (unoccupied grid) (Jung et al., 2016). A user-defined grid cell size ($g$) is used here to divide the space into small cells. Finer grids generally result in more realistic representation of objects and thus a more accurate driver viewshed since they can account for smaller objects. However, selecting a small grid cell size may cause higher computational costs, i.e., processing time. The relationship between the grid cell size and the processing time will be explored in Section 5.3.

Fig. 3 illustrates a driver location, line of sight, and object points on the grid representation. Prior to the viewshed analysis, users need to define the driver's horizontal viewing angle to narrow down the effective visible area when looking straight ahead. (Section 5.2.2 evaluates the selection of this horizontal viewing angle in more detail). The grid cells on the outer edge of the grid map within the driver's horizontal viewing angle are initially considered as the ends of the driver's view point. Subsequently, the line of sight starts from the driver location and extends as a ray to each outer cell. Grid cells on the line of sight are then recognized using the Bresenham's algorithm (Joy, 1999), which identifies cells within a grid that formulate an approximation of a straight line. The indices of these designated grid cells for the line are stored and used to retrieve the points within them. The algorithm visits all the driver's view points within the pre-defined horizontal viewing angle (e.g., 120° in Fig. 3), and non-visible space blocked by obstructions are investigated. The details of the detection of obstruction in the line of sight will be intensively discussed in the following section.

### 3.3. Detection of obstruction

Considering the 3D object points on the line-of-sight path, non-visible space blocked by obstructions and visible space can be separated. Fig. 4a describes how to determine whether an object constitutes as a sight obstruction in a profile view. The vertical distance ($\Delta z$) between each object point and the line of sight is calculated as

$$\Delta z = |\{z_d - \Delta h \tan(\theta°)\} - z_o| \quad (1)$$

if $\Delta z \leqslant g/2$, the view point is obstructed


**Fig. 3.** Retrieval of object points using the line-of-sight analysis. Ground points are omitted for clarity.

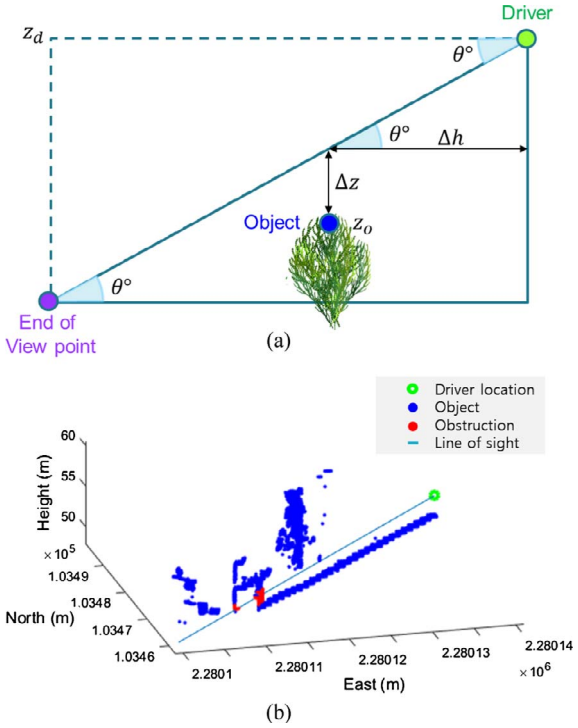


**Fig. 4.** Concept of the detection of and obstruction in a line-of-sight path: (a) extracted object points in a line-of-sight path and (b) detection of obstruction.

where $z_d$ is the driver height, $\Delta h$ is the horizontal distance between the driver location and the object point, and $\theta°$ is the driver's vertical viewing angle (in degrees) to the end of view point. Since detection of obstruction is conducted using z-values without grid discretization, half the user-defined grid cell size ($g/2$) is assumed and used as a criterion: if the $\Delta z$ is equal to or less than $g/2$, the object point is considered an obstruction that would block the driver's view of the road. This process operates recursively until all the object points on the line-of-sight path are evaluated. Fig. 4b shows an example of obstruction detection, where the driver's line of sight passing below the tree canopy is finally blocked by another object. Subsequently, only the space closer than the obstruction

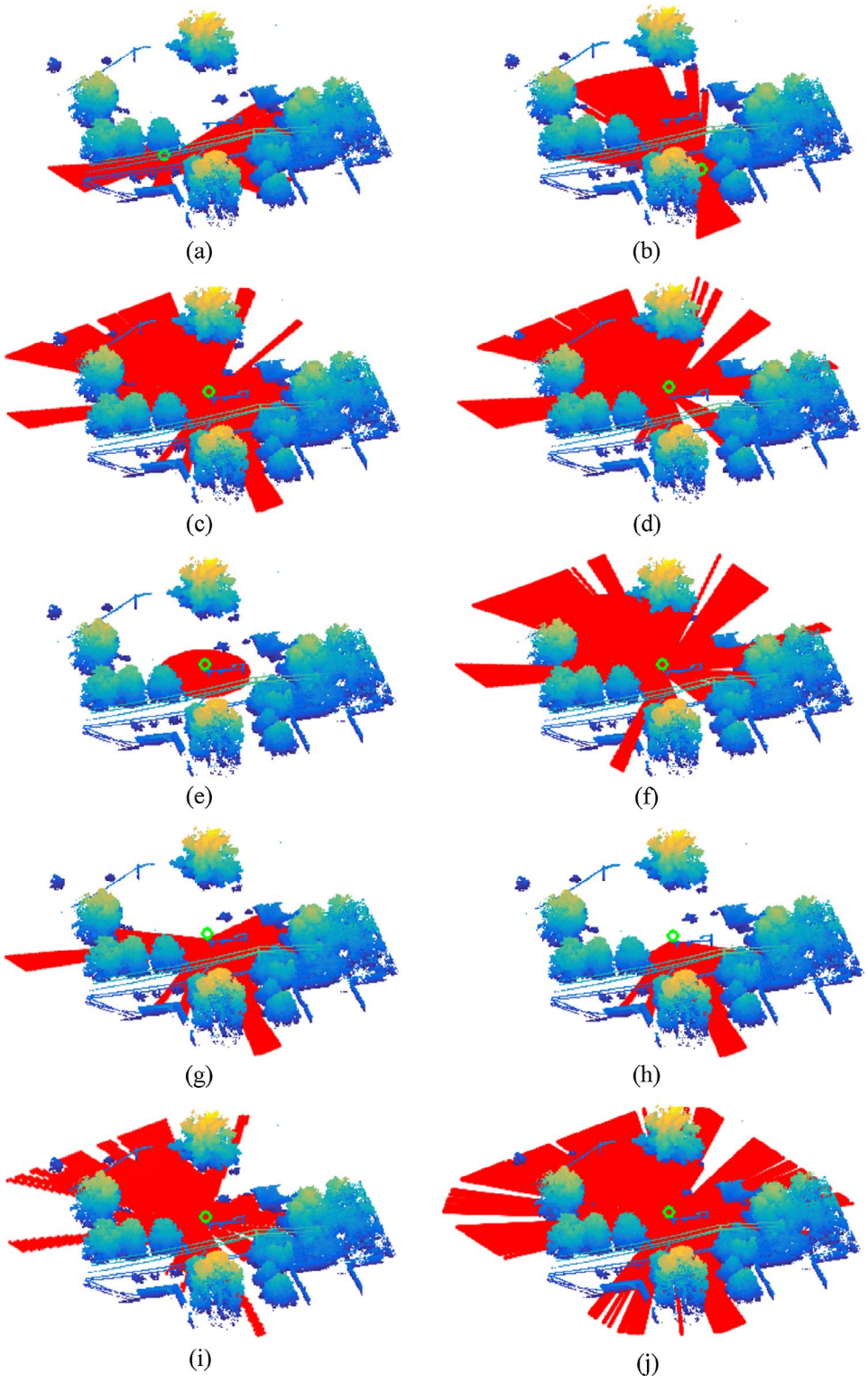


**Fig. 5.** Examples of changes in the viewshed resulting from different driver conditions. The green dot indicates driver's location and red dots indicate the driver's viewshed: (a) eastbound approach; (b) northbound approach; (c) passenger car (1.067 m); (d) heavy vehicle (2.316 m); (e) vertical viewing angle of −5°; (f) vertical viewing angle of +5°; (g) horizontal viewing angle of 240°; (h) horizontal viewing angle of 120°; (i) grid cell size of 1 m; and (j) grid cell size of 0.1 m. (For interpretation of the references to colour in this figure legend, the reader is referred to the web version of this article.)

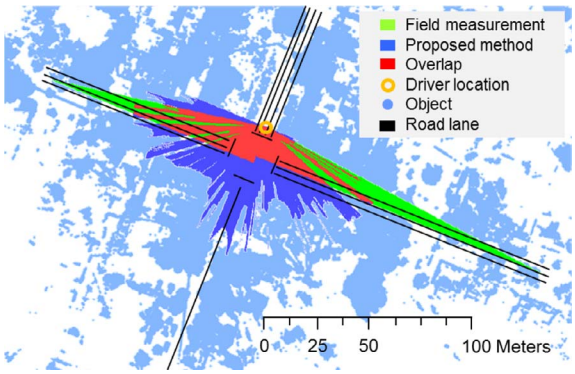


**Fig. 6.** Comparison of visible areas estimated by the field measurement and the proposed method.

nearest to the driver's location is kept as a part of the driver's viewshed.

The flexibility of the proposed simulation enables evaluation of the visibility of different driver positions (e.g., different lane or motion), heights, vertical/horizontal viewing angles, and resolutions. Fig. 5 illustrates such examples in 3D views. Fig. 5a and b show differences in visibility depending on where the car is located, Fig. 5c and d show differences in driver height, Fig. 5e and f alternate the vertical viewing angle to show differences if the driver is looking down on the road or up at a traffic signal, Fig. 5g assumes the driver is rotating their head, Fig. 5h models peripheral vision, and Fig. 5i and j consider the influence of the analysis resolution. This versatility is of great advantage for effective evaluation of several different traffic motions. Another advantage is that one can consider multi-modal forms of transportation such as pedestrians and bicyclists. A few common scenarios will be evaluated in the Section 5 by varying the parameters representing the driver's conditions.

### *3.4. Comparison with field measurements*

A comparison of the algorithm-generated viewshed and the conventional field measurements is conducted to reveal how the proposed methodology provides significantly more detail for the visible area. For that purpose, the sight triangles developed from the field measurements are rasterized using the grid cell size defined in the previous rasterization phase. Subsequently, as shown in an example of Fig. 6, the estimated driver's 3D viewshed is projected on the visible scene determined by the field measurements to compare the detail visibility. Further, for quantitative comparison, the degree of overlap between two visible areas is calculated, pixel-by-pixel.

## 4. Case study

### *4.1. Description of the intersection*

The signalized, four legged intersection of SW Jefferson Way and SW 9th Street (Fig. 7a) is located in Corvallis, Oregon. SW Jefferson Way runs approximately east-west while SW 9th Street runs approximately north-south. Fig. 7b displays the geometry of the intersection SW Jefferson Way. The northbound approach along SW 9th Street consists of a single shared left/through/right turn lane.


**Fig. 7.** Intersection of SW Jefferson Way and SW 9th Street: (a) intersection image obtained from Google maps and (b) intersection geometry.

**Table 2**
SW Jefferson Way at SW 9th Street SD analysis summary.

| Approach | Stopping sight distance (ft) | | | Intersection sight distance (ft) | | |
|---|---|---|---|---|---|---|
| | Required* | Calculated | Measured | Required* | Calculated | Measured |
| Northbound | 155 | 151.86 | 279 | 275.6 | 275.63 | 294 |
| Southbound | 155 | 151.86 | 681 | 275.6 | 275.63 | 330 |
| Eastbound | 155 | 151.86 | 633 | 275.6 | 275.63 | 217 |
| Westbound | 155 | 151.86 | 681 | 275.6 | 275.63 | 459 |

* Based on a 25 mph design speed (AASHTO, 2011).

The southbound approach along SW 9th Street consists of an exclusive right turn lane and a shared through/left turn lane, separated by an exclusive marked bicycle lane. This intersection was selected for the case study due to the proximity and size of fixed objects near the corners of the intersection that present intersection SD obstructions. Examples of obstructions at this site include vegetation, both trees and shrubbery, utility poles and traffic signal cabinets, on-street parallel parked cars, and the placement of buildings.

### 4.2. Conventional field measurements

Table 2 provides the SD analysis summary for the study conducted at SW Jefferson Way and SW 9th Street. The required SSD and ISD measurements are based on requirements provided by American Association State Highway and Transportation Officials (AASHTO) for a design speed of 25 mph (AASHTO, 2011). The ISD for each approach is the smallest distance measured to the right following AASHTO recommendations. The smallest measurement is used for the purpose of being conservative thereby promoting intersection safety. Furthermore, AASHTO (2011) states "if the available ISD for an entering or crossing vehicle is at least equal to the appropriate SSD for the major road, then drivers have sufficient SD to anticipate and avoid collisions". This is the case for all ISD measurements when compared to the required and calculated SSD at the case study intersection. However, this is not the case when compared with the measured SSD. Based on the data collected, the intersection has sufficient SSD and ISD for nearly all approaches; however, the eastbound approach does not provide adequate ISD and would require mitigation of the intersection obstructions to meet the AASHTO requirements for ISD. Fig. 8a shows a typical setup during the field campaign and Fig. 8b shows an example of resulting SD triangles overlain on aerial imagery.

### 4.3. Point cloud data collection

Lidar point cloud data for the intersection were acquired at the intersection from 12 independent setups strategically positioned throughout the scene. Each scan captured a 360° panorama of the scene, with a sampling resolution of 0.05°. A Trimble R8 GNSS Receiver was mounted to the top of the scanner to provide geodetic positioning. GNSS data were collected using RTK correctors from the Oregon Real Time GNSS Network (ORGN), which is managed by Oregon DOT.

To register the several scans captured from different positions into a single point cloud, 6″ Black and White checkerboard patterned targets were spread across the scene to serve as tie points. The center points of these targets were captured using a reflectorless total station sighted on the center of each target. These target centers were then linked to ground control points by positioning a 360° prism mounted on top of a rod placed on the ground control points. Geodetic coordinates for the ground control points were also obtained using the ORGN. The registration process was completed in Leica Cyclone 9.0 software. In addition to utilizing the targets for the registration, cloud to cloud surface matching techniques were utilized to help improve the fit between overlapping scans. The registered point-cloud data was resampled to point spacing of 2 cm as well as edited to remove noise due to passing vehicles and


**Fig. 8.** Southbound approach SSD triangles of intersection of SW Jefferson Way and SW 9th: (a) SSD study in progress and (b) SSD triangles overlain on Arcmap image.

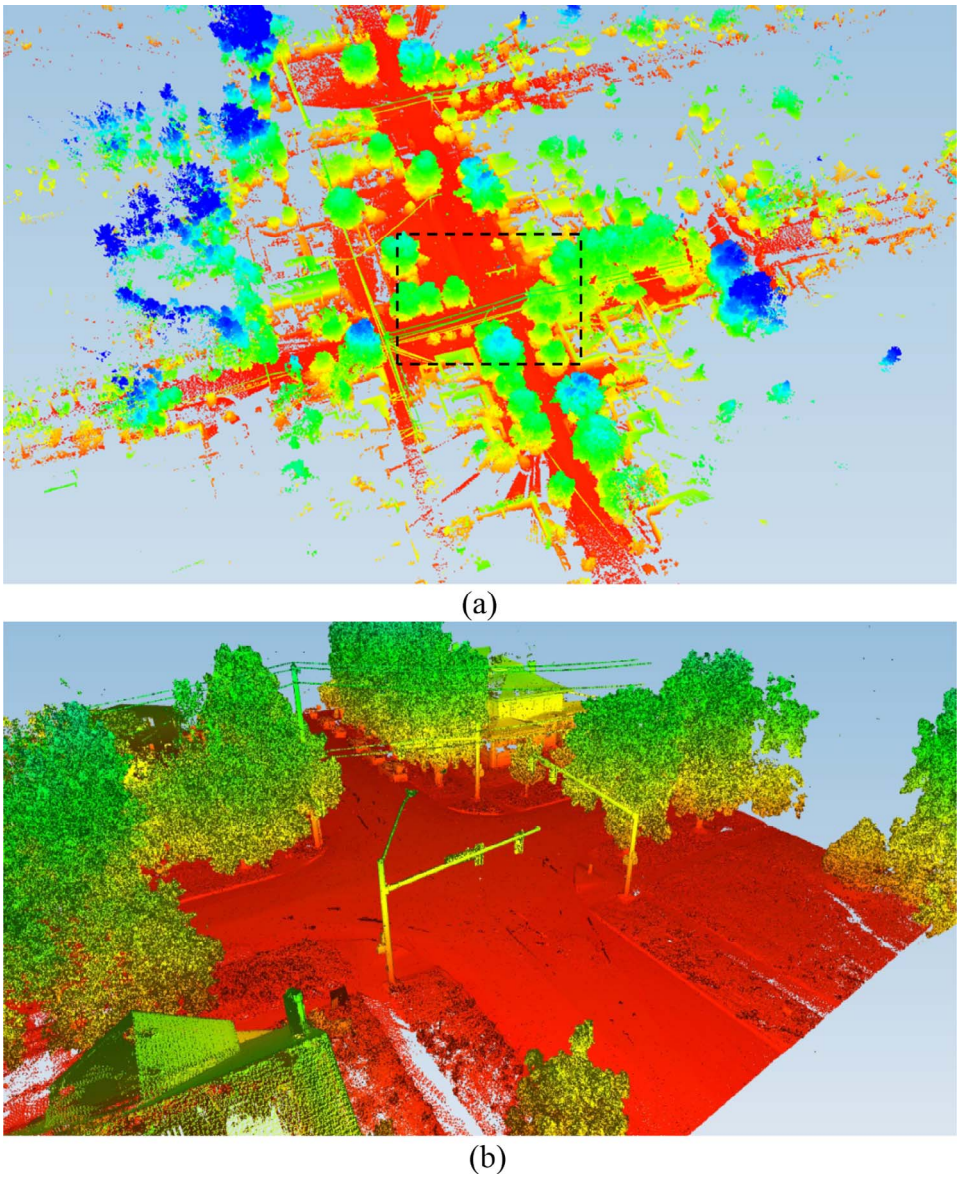


**Fig. 9.** Point cloud data obtained for the intersection (47.7 million points): (a) overview and (b) close-up view of intersection.

pedestrians since they do not represent static objects at the scene that should be considered in the site analysis. In total, the resulting point cloud contained approximately 47.7 million scan points. Fig. 9a shows the entire point-cloud data colored by height variations and Fig. 9b shows the intersection in close-up view.

## 5. Simulation and results

### *5.1. Comparison of simulation results with conventional measurements*

The simulated driver's viewsheds from the four different intersection approaches at SW Jefferson Way and SW 9th Street are represented in Fig. 10. The simulated 3D viewsheds were projected in an x-y plane to compare their detail visibility with the 2D field measurements as well as to calculate the overlap rate. For each approach, the driver's horizontal and vertical viewing angles were fixed with constant values of 180 and $-1^{\circ}$, respectively. Additionally, the vehicle type was assumed to be a passenger car located in the right lane. The proposed method provides significantly more detail than conventional measurements (Fig. 10) because the conventional approach has been based on a relatively few discrete measurements without considering detailed objects in 3D. As a result, the conventional analysis over predicted visible areas to the driver that an obstruction would block. In contrast, the proposed simulation could incorporate a variety of objects to the virtual 3D scene and evaluate their impacts on available SD. Another

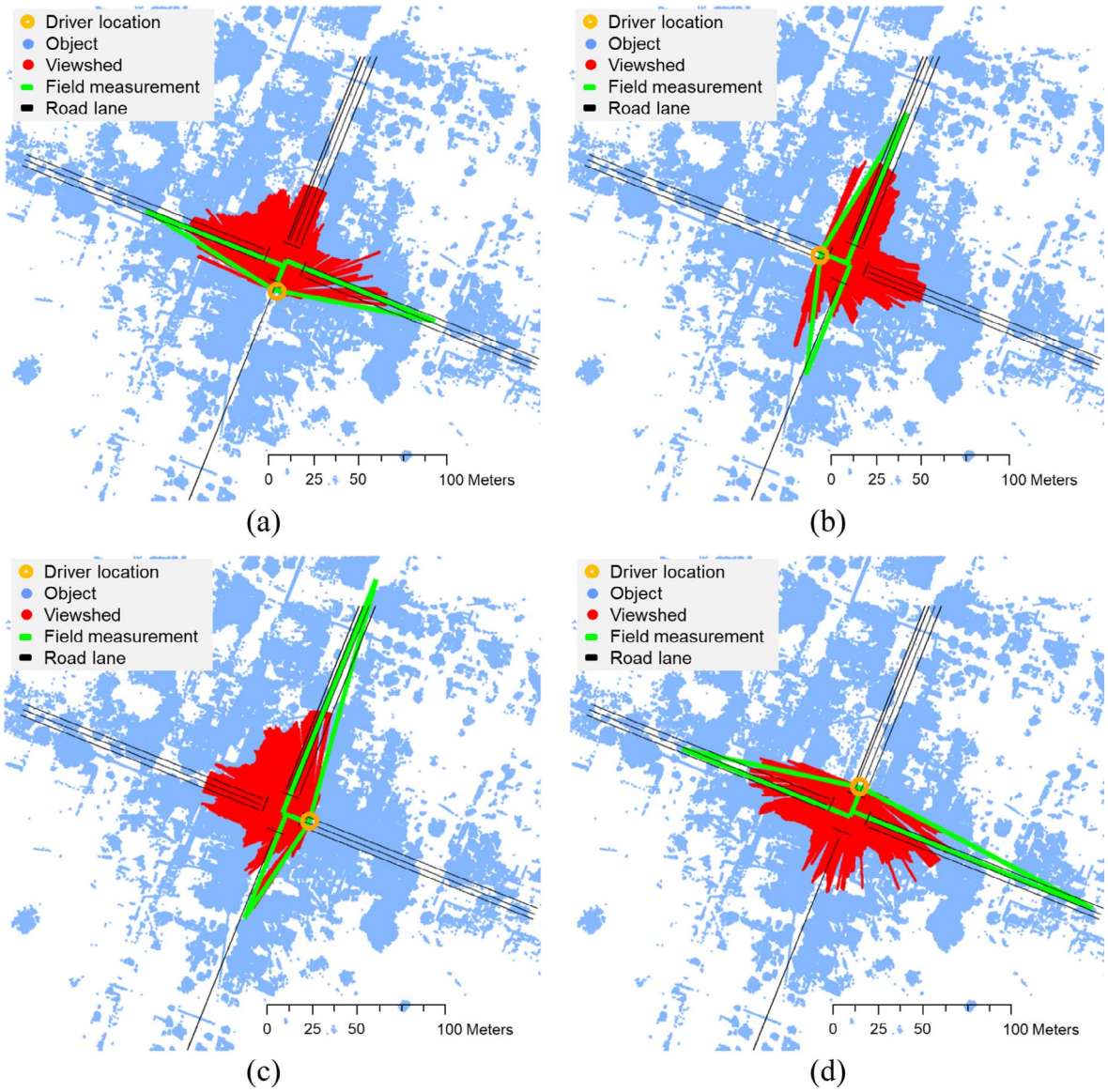


**Fig. 10.** Comparison of visibility between algorithm-generated results and conventional field measurements in four different approaches at intersection: (a) northbound approach (overlap 61.6%); (b) eastbound approach (overlap 68.2%); (c) westbound approach (overlap 51.2%); and (d) southbound approach (overlap 51.7%).

limitation of the conventional analysis is that cones are commonly placed at the center or shoulder of the road to improve the safety of technicians and minimize the impact on traffic. Hence, they are offset from the actual location of the driver, immediately introducing a bias into the analysis. It is further shown that different approaches yield different overlap rates, ranging from 51.2 to 68.2%. The lowest overlap rate was found on the south approach due to the over-predicted visible area of the right triangle.

### *5.2. Investigation of potential scenarios*

#### *5.2.1. Impact of driver height*

A key advantage of the proposed method is that it enables rapid simulation of multiple transportation user scenarios. Hence, the designer can consider a wider range of possibilities as compared to the conventional method. One example is varying the driver height, which can significantly influence the length of visible roadway. In this scenario, the impact of driver height was simulated by increasing the driver height from 1.0 m to 2.5 m, with a constant interval of 0.5 m. The driver's horizontal and vertical viewing angles were fixed with 180 and $-1^{\circ}$, respectively, and the driver's location was assumed to be in the right lane of the southbound approach. Visibility changes significantly depending on the driver height (Fig. 11). The maximum extent of the visible area and overlap rate increased until the driver height reached 2.0 m, after which the overlap rate showed a sharp decrease at 2.5 m. This likely occurred

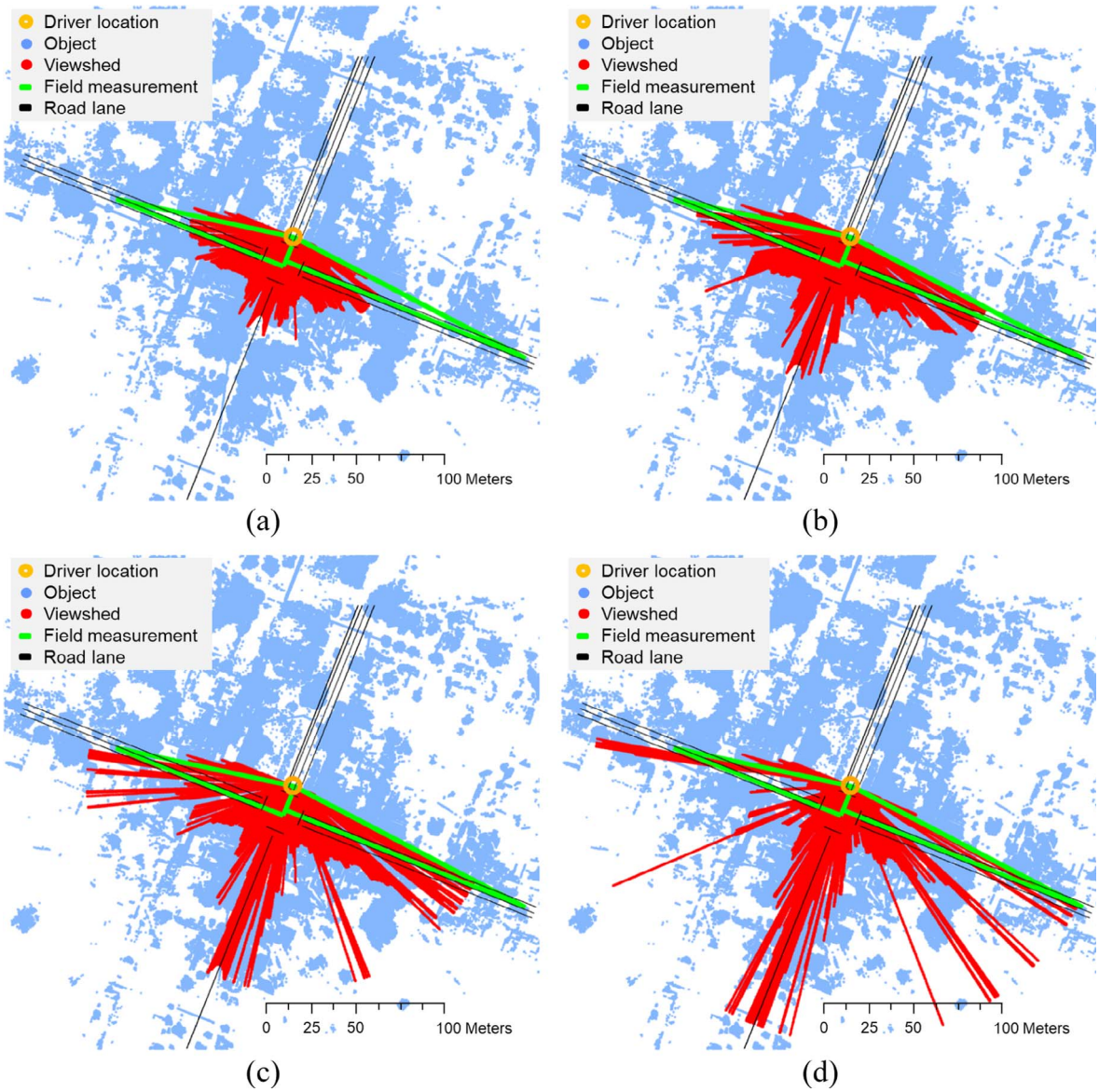


**Fig. 11.** Impact of driver height on visibility: (a) 1.0 m (overlap 48.8%); (b) 1.5 m (overlap 64.3%); (c) 2.0 m (overlap 70.1%); and (d) 2.5 m (overlap 51.7%).

because the driver's lines of sight were blocked by some tall artifacts or tree branches, which is not well reflected by conventional field measurements.

### *5.2.2. Impact of horizontal viewing angle*

The influence of visual attention on the driving task is significant, as it has been proposed that 90% of the driving task is visually controlled (Hartman, 1970; Hills, 1980; Sivak, 1996). Recarte and Nunes (2000) found mean vertical visual fixation to be 1° below the horizon with a ± 1° standard deviation. Meanwhile, AASHTO (2010) found the horizontal viewing angle can vary depending on driver's awareness. It is therefore desirable to simulate the impact of different horizontal viewing angles on the visible area. In this scenario, the vertical viewing angle was fixed with constant value of −1° and the vehicle type was assumed to be a passenger car in the right lane of south approach. While looking straight ahead, objects within 180° of horizontal view can be seen (Fig. 12a), but the information is not consciously processed by the driver. The useful field of horizontal view in which drivers are aware of visual information ranges from 20 to 30°, which were simulated as shown in Fig. 12b and c, respectively. Compared with the full horizontal view (180°), one can see that the visibility has been significantly reduced. Further, the low overlap rates (3.8 and 2.6%) indicate the conventional method can be problematic for handling diverse conditions. Finally, objects can be seen in high resolution within 4° of the horizontal view (Fig. 12d).

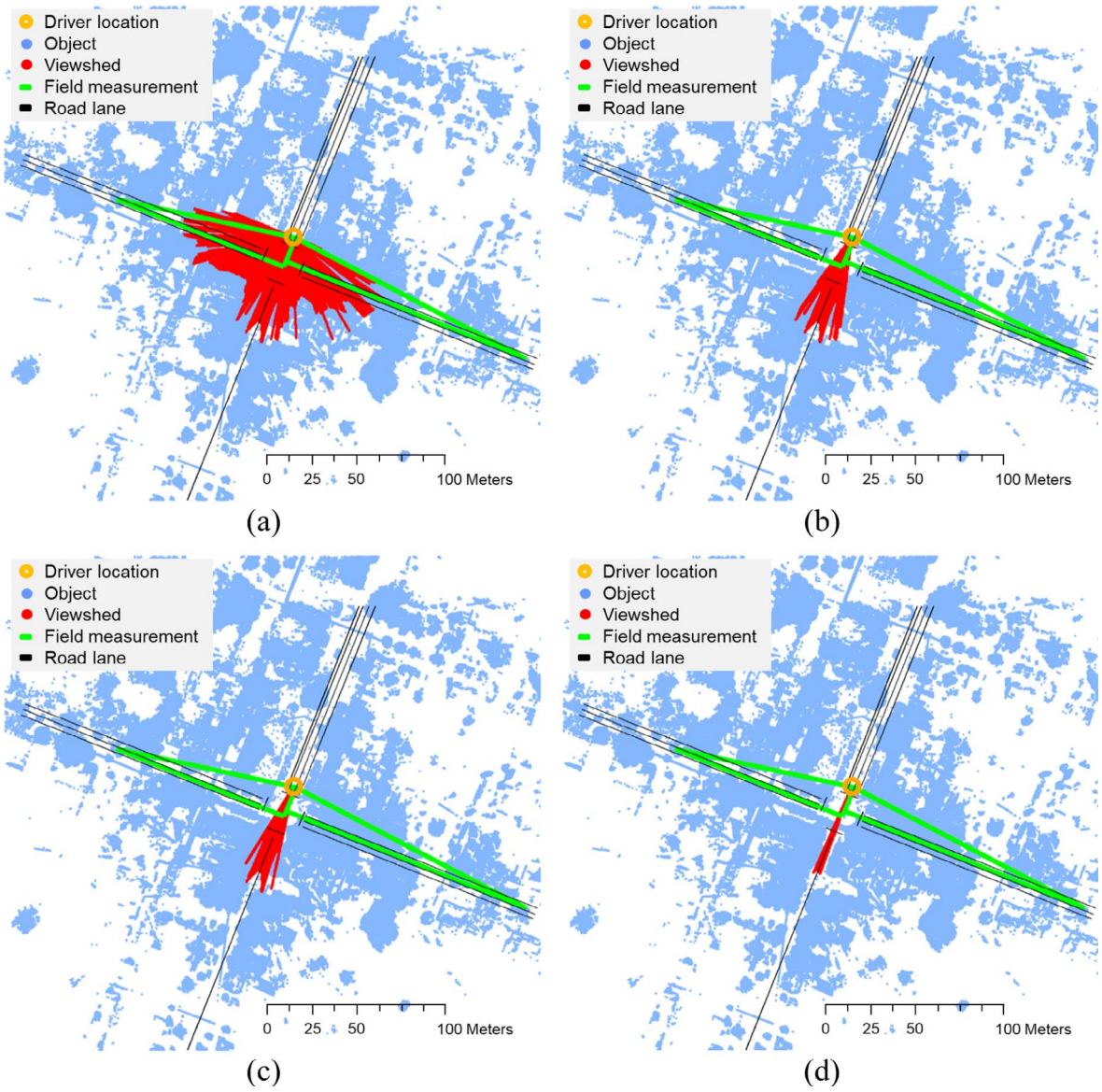


**Fig. 12.** Impact of driver's horizontal viewing angle on visibility: (a) 180° full horizontal view (overlap 51.7%); (b) 30° maximum useful field of view (overlap 3.8%); (c) 20° minimum useful field of view (overlap 2.6%); and (d) 4° accurate vision (overlap 0.6%).

### *5.2.3. Dynamic motion*

The proposed method is also particularly useful in simulation of driver's dynamic motion. Fig. 13 illustrates an example of a passenger car performing a right turn from the right-turn lane of the southbound approach. The other driver's horizontal and vertical viewing angles were fixed at 180 and −1°, respectively. The dynamic motion was modeled as a simple circular curve and recorded with the constant interval of 10° (Fig. 13a). The variations in driver's visibility were obtained (Fig. 13b–f), which demonstrated the great potential utility of the proposed simulation.

### *5.2.4. Transportation modes*

In this phase, the visibility of different vehicle types and modes including bicyclists and pedestrians were simulated. For realistic visualization, the generated viewsheds in grid format were converted to a polygon format and imported into commercial ArcGIS software. This process was completed by exporting a point (centroid) for each grid cell that is visible and then converting those combined points into a single polygon that bounds those points. Fig. 14 represents the viewsheds of different transportation modes overlain on an orthoimage in ArcMap. The viewsheds of the passenger car and the heavy vehicle were simulated in the right-turn lane of the southbound approach, while the bicyclist was simulated in the bike lane, and the pedestrian was simulated on the sidewalk. For all modes, the horizontal and vertical viewing angles were assumed to be 180° and −1°, respectively.

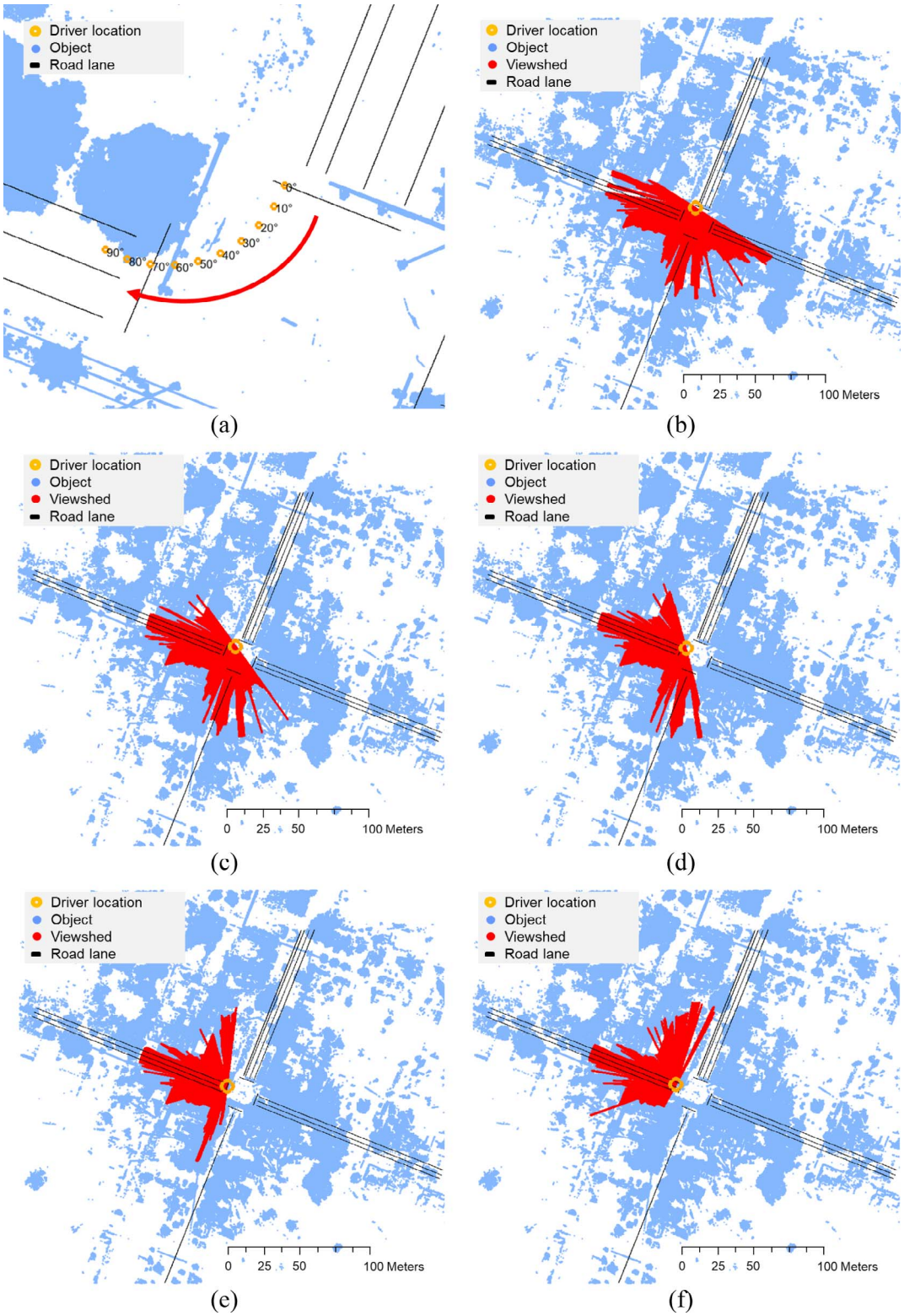


**Fig. 13.** Variations in driver's visibility in dynamic motion: (a) vehicle path; (b) 10°; (c) 30°; (d) 50°; (e) 70°; and (f) 90°.

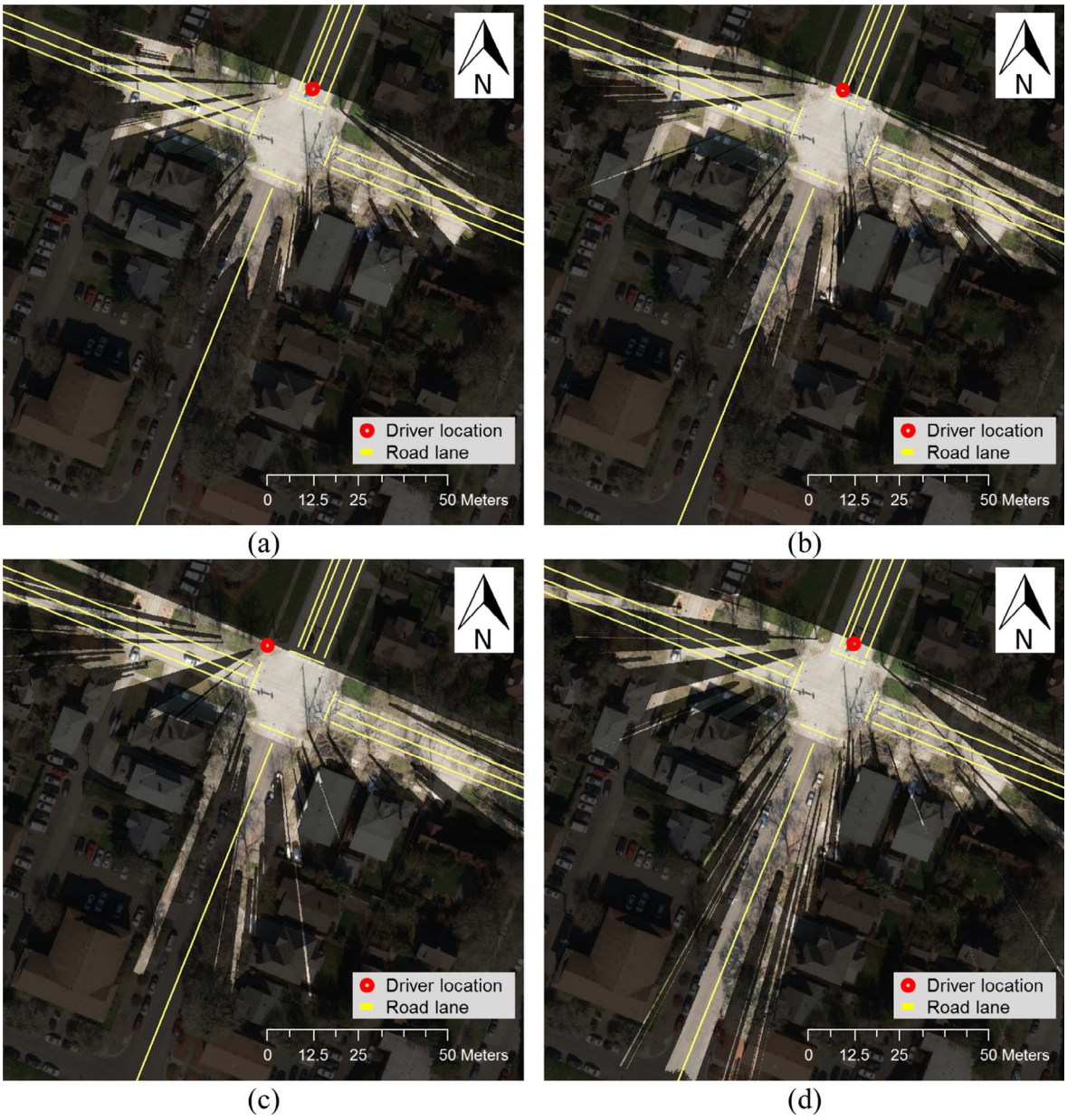


**Fig. 14.** Variations in driver's visibility according to different transportation modes. Bright regions indicate visible area: (a) passenger car (1.067 m) (overlap 51.7%); (b) bike (1.372 m) (overlap 55.3%); (c) pedestrian (1.70 m) (overlap 52.3%); and (d) heavy vehicle (2.316 m) (overlap 59.1%).

### *5.2.5. Application to authorities*

Within sight triangles, any objects above the height of the adjacent roadway that has the potential to obstruct the driver's view should be removed or lowered (AASHTO, 2011). Fig. 15 shows a potential use of the generated 3D viewshed to detect the obstructions within the sight triangles. In this example, the vehicle type was assumed to be a passenger car (1.067 m) in the right lane of south approach, and the driver's horizontal and vertical viewing angles were fixed at 180 and $-1^{\circ}$, respectively. The obstructions that block the driver's view (e.g., tree trunks and traffic signal poles), were detected by Eq. (1) and projected onto the x-y plane. Subsequently, all of the points that fall within the same grid cells were highlighted in red, which could help maintenance personnel identify intersection obstructions and make informed management decisions. These decisions could be as simple as removing minor vegetation or as complex as intersection realignment depending on the severity of the obstructions. Further, the virtual environment allows one to model potential maintenance procedures in the point cloud and evaluate the improvement on intersection visibility to determine an optimal cost-benefit ratio. For example, one can remove portions of the point cloud corresponding to an obstructing tree, re-run the analysis, and compare the new viewshed with the current conditions to evaluate whether the cost of removal produces a significant gain in visibility. Then once the optimal maintenance procedure is determined, it can be completed by the maintenance crews.

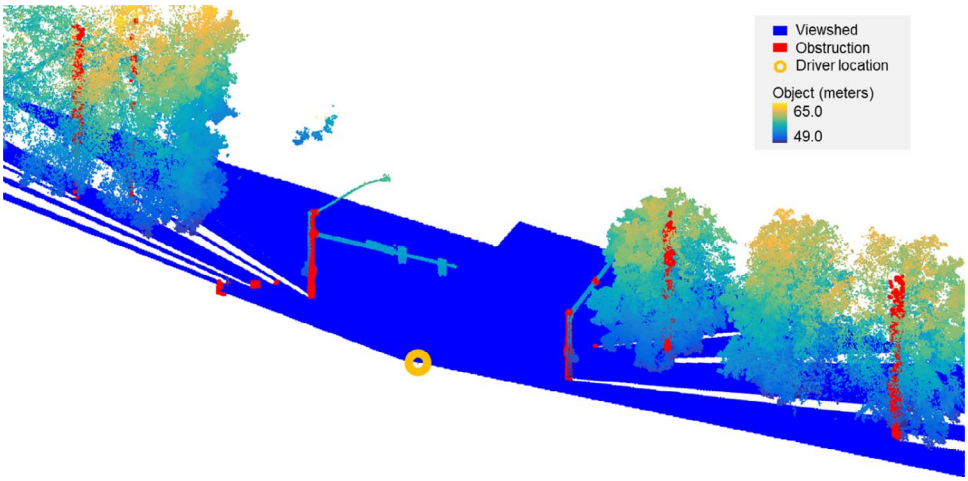


**Fig. 15.** Intersection obstructions detected by generated 3D viewshed within the sight triangles.

### 5.3. Impact of grid size on processing time

In this section, the impact of grid size on the runtime of the proposed methodology was compared with the authors' previous work, the voxel-based method (Olsen et al., 2015). Both algorithms were implemented in the Matlab environment, and simulated on a computer with Intel® Xeon® processor (2.4 GHz, 24.0 GB of RAM). Note that the comparison was conducted using the reduced number of scan points (approximately 1.2 million points) due to the excessive processing time of the voxel-based method on the larger 47.7 million point dataset.

As anticipated, the test (Fig. 16) indicated that the runtime increases as finer grid sizes were used. Notably, the increase in the runtime of the voxel-based method was very significant as the grid size decreased: it grew exponentially and jumped up to 6478.3 s with the grid size of 0.2 m. In contrast, the impact of grid size on the runtime of the proposed method was not as significant as the voxel-based method; the runtime grew relatively slowly with decreasing the grid size and yielded only 180.7 s even with the grid size of 0.1 m. This is due to the fact that the voxel-based method is inefficient for sparse and unbalanced distribution of scan points by assigning pointers to 3D voxels where no point exists, and thus it used more memory and time than was required (Han et al., 2012). On the other hand, the improved query performance was achieved with the proposed method because the operations for finding scan points and detecting obstructions were separated on the 2D grid space and the 1D vertical space, respectively. As the processing time reduced, the angular resolution parameter of the voxel-based method, which was used to limit the search space for obstructions, is no longer used in this method. As can be seen in Fig. 17, despite an overall improvement in processing speed, the proposed method showed almost the same performance of viewshed estimation as that of the voxel-based method: the overlap rate was calculated to be 95.6%. The small difference was due mainly to the obstruction detection in a line-of-sight path: while the voxel-based method detects

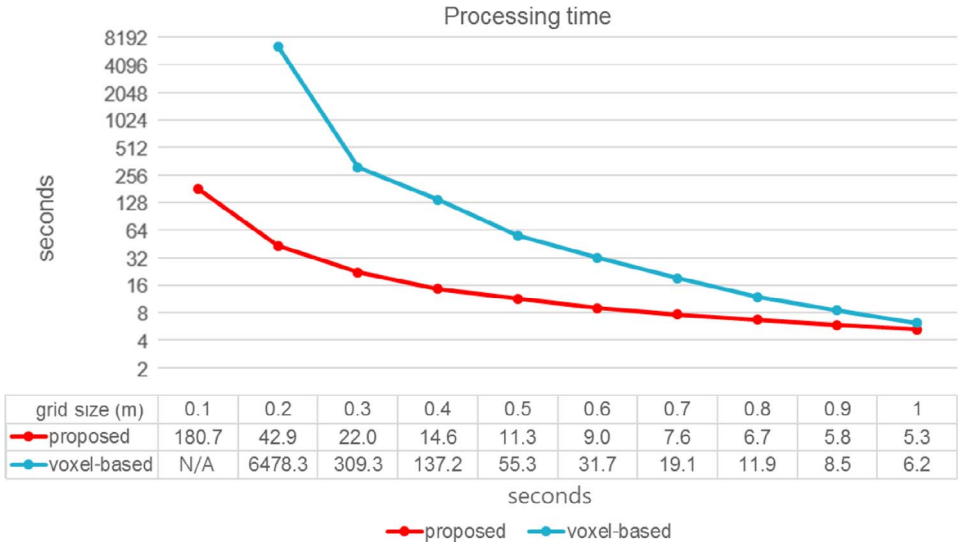


| grid size (m) | 0.1 | 0.2 | 0.3 | 0.4 | 0.5 | 0.6 | 0.7 | 0.8 | 0.9 | 1 |
|---|---|---|---|---|---|---|---|---|---|---|
| proposed | 180.7 | 42.9 | 22.0 | 14.6 | 11.3 | 9.0 | 7.6 | 6.7 | 5.8 | 5.3 |
| voxel-based | N/A | 6478.3 | 309.3 | 137.2 | 55.3 | 31.7 | 19.1 | 11.9 | 8.5 | 6.2 |

**Fig. 16.** Comparison of processing time between the voxel-based and the proposed methods with a reduced data set (1.2 million points).

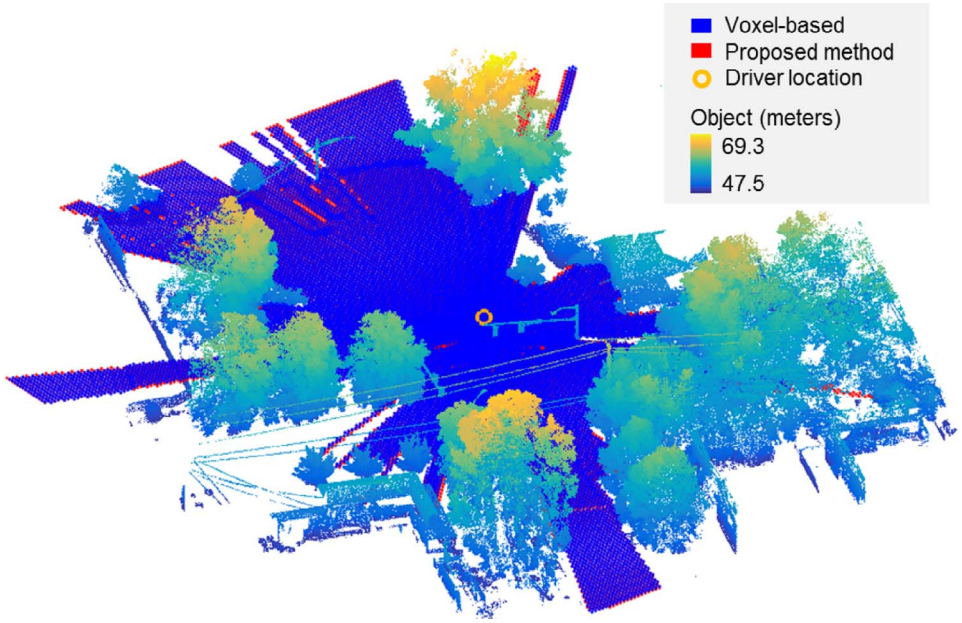


**Fig. 17.** Comparison of generated 3D viewshed between the voxel-based and the proposed methods with reduced data set (1.2 million points).

obstructions in a line of sight voxels, the proposed method detects obstructions by calculating the vertical distance between each object point and the line-of-sight path.

With the grid cell size of 0.1 m, the proposed method resulted in reasonable runtime (approximately 3 h) using the 44.7 million points obtained in the study site. A finer grid size could also be used, but the amount of accuracy improvement will be relatively minor and likely not worth the significant increase the required algorithm runtime. Therefore, the grid cell size of 0.1 m has been used in the other steps of this research.

## 6. Conclusions

In this paper, a novel approach to perform sight distance analysis was developed using 3D lidar data, which improves upon the existing 2.5D approaches. This algorithm simplifies the data into a grid form for efficiency but still preserves the 3D nature of the scene. The approach also enables the user to evaluate visibility from a variety of perspectives throughout the scene. This flexibility enables the algorithm to successfully evaluate SD constraints from a variety of vehicles, driver heights, viewing angles as well as multi-modal forms of transportation. The algorithm can handle complex objects throughout the scene and showed several benefits over conventional measurements. First, data can be collected safely from the side of the road or from a mobile platform (MLS) moving with traffic. Second, more detail on the road and obstructions are collected and can be considered in the visibility analysis. Third, it provides more flexibility in evaluating various transportation modes, including multi-modal transportation, which is becoming increasingly important to reduce congestion in urban areas and promote public health and safety. Fourth, the conventional method significantly overestimated the visible portion of the intersection, which can lead to unsafe intersections being considered safe but do not provide adequate SD. Fifth, the algorithm-generated viewshed can be simply exported as polygons and used in GIS tools, which enables users to extend the application of the simulation result and consider it in context with other important data in the safety evaluation. Sixth, the viewshed enables maintenance personnel to easily identify intersection obstructions and evaluate alternatives of improvements, thus aiding their decision making processes. Further, in comparison with a 3D voxel method, the proposed method is significantly more computationally efficient and requires fewer parameters (height interval and grid size).

However, there are two challenges associated with the proposed methodology. Although the study intersection is an authentic real-world example intersection, more complex intersections should be considered in future work; for example, the integration of ground filtering into the proposed pipeline to enable the algorithm to work on intersections located in hilly terrain. For the obstruction detection on a line-of-sight path, a simplified approach using half the user-defined grid cell size was assumed and adopted as a criterion. Nevertheless, more rigorous mathematical criteria accounting for the divergence of the view cone would be beneficial in improving the proposed sight distance analysis, particularly at far distances.

In future work, the automated classification of detected obstructions (e.g., pole or tree) could enhance authorities' decision making since some objects may not be removable. Future work could also consider the 4D dynamic motions of the driver as well as other objects in the scene to identify additional conflicts or perform more advanced statistical analysis. Such a capability will enable design and maintenance engineers to consider the visibility of passing vehicles under various traffic conditions such as different speeds, restricted SD due to oncoming or impeding vehicles, etc.

## Acknowledgements

This work has been funded by the US Department of Transportation's University Transportation Center Program, Grant # DTRT13-G-UTC40 through the Pacific Northwest Regional University Transportation Center (PacTrans) and the National Science Foundation Award CMMI 1351487. Leica Geosystems and David Evans and Associates provided equipment and software utilized in this study. Maptek I-Site also provided software utilized for this study. Matt O'Banion assisted with the field data collection.

## References

AASHTO, 2010. Highway Safety Manual, first ed. American Association of State Highway and Transportation Officials, Washington, DC.
AASHTO, 2011. A Policy on Geometric Design of Highways and Streets, 2011. American Association of State Highway Transportation Officials, Washington, DC.
Ai, C., Tsai, Y.J., 2016. An automated sign retroreflectivity condition evaluation methodology using mobile LIDAR and computer vision. Transport. Res. Part C: Emerg. Technol. 63, 96–113.
Batchelor, J.L., 2016. Quantification of Ecological Change Using Repeat Photography and Ground Based Lidar, Forest Ecosystems and Society. Oregon State University, pp. 219.
Brown, A., Brennan, S., 2015. Simulating vehicle dynamics on both design plans and laser-scanned road geometry to guide highway design policy. Transport. Res. Part C: Emerg. Technol. 50, 28–36.
Castro, M., Anta, J.A., Iglesias, L., Sánchez, J.A., 2014. GIS-based system for sight distance analysis of highways. J. Comput. Civil Eng. 28 (3), 04014005.
Castro, M., De Santos-Berbel, C., Iglesias, L., 2017. A comprehensive methodology for the analysis of highway sight distance. In: Proceedings in the CitA BIM Gathering Conference on Transport Infrastructure and Systems. CRC Press, Rome, Italy, pp. 193–199.
Castro, M., Iglesias, L., Sánchez, J.A., Ambrosio, L., 2011. Sight distance analysis of highways using GIS tools. Transport. Res. Part C: Emerg. Technol. 19 (6), 997–1005.
Che, E., Olsen, M.J., 2017. Fast ground filtering for TLS data via Scanline Density Analysis. ISPRS J. Photogramm. Remote Sens. 129, 226–240.
De Santos-Berbel, C., Castro, M., Medina, S.L.-C., Paréns-González, M., 2014. Sight distance studies on roads: influence of digital elevation models and roadside elements. Procedia-Soc. Behav. Sci. 160, 449–458.
Delaunay B.N., 1934. Sur la sphère vide. Izvestia Akademii Nauk SSSR, Otdelenie Matematicheskikh i Estestvennykh Nauk 7, 793–800.
Fambro, D.B., Fitzpatrick, K., Koppa, J.R., 1997. Determination of Stopping Sight Distances. Transportation Research Board National Research Council, Washington, D.C.
Han, S., Cho, H., Kim, S., Jung, J., Heo, J., 2012. Automated and efficient method for extraction of tunnel cross sections using terrestrial laser scanned data. J. Comput. Civil Eng. 27 (3), 274–281.
Hartman, E., 1970. Driver visual requirements. Proceedings in the International Automobile Safety Conference. Society of Automotive Engineers, New York, USA.
Hassan, Y., Easa, S.M., Abd El Halim, A.O., 1996. Analytical Model for Sight Distance Analysis in 3D Highway Alignments. Transportation Research Board, Washington, DC.
Hills, B.L., 1980. Vision, visibility, and perception in driving. Perception 9 (2), 183–216.
Ismail, K., Sayed, T., 2007. New algorithm for calculating 3D available sight distance. J. Transp. Eng. 133 (10), 572–581.
Jha, M., Karri, G., Kuhn, W., 2011. New three-dimensional highway design methodology for sight distance measurement. Transport. Res. Record: J. Transport. Res. Board (2262), 74–82.
Jha, M.K., Karri, G.A., 2009. Road surface development and sight distance calculation with new visualization methods. In: Proceedings of the 2nd WSEAS International Conference on Sensors and Signals: Sensors, and Signals and Visualization, Imaging and Simulation and Materials Science, pp. 220–225.
Joy, K.I., 1999. Breshenham's Algorithm. Computer Science Department, University of California, Davis.
Jung, J., Hong, S., Yoon, S., Kim, J., Heo, J., 2016. Automated 3D wireframe modeling of indoor structures from point clouds using constrained least-squares adjustment for as-built BIM. J. Comput. Civil Eng. 30 (4), 04015074.
Jung, J., Stachniss, C., Kim, C., 2017. Automatic room segmentation of 3D laser data using morphological processing. ISPRS Int. J. Geo-Inf. 6 (7).
Khattak, A., Hallmark, S., Souleyrette, R., 2003. Application of light detection and ranging technology to highway safety. Transport. Res. Rec.: J. Transport. Res. Board 1836, 7–15.
Khattak, A.J., Shamayleh, H., 2005. Highway safety assessment through geographic information system-based data visualization. J. Comput. Civil Eng. 19 (4), 407–411.
Mallela, J., Mitchell, A., Gustafson, J., Olsen, M.J., Parrish, C., Gillins, D., Kumpula, M., Roe, G.V., submitted for publication. Effective Use of Geospatial Tools in Highway Construction. U.S. Department of Transportation.
Marinelli, G., Bassani, M., Piras, M., Lingua, A.M., 2017. Mobile mapping systems and spatial data collection strategies assessment in the identification of horizontal alignment of highways. Transport. Res. Part C: Emerg. Technol. 79, 257–273.
McKinley, L., 2014. Sight Distance Standards and Deviations for Highway Approaches. Oregon Department of Transportation.
Olsen, M.J., 2013. Guidelines for the Use of Mobile LIDAR in Transportation Applications. Transportation Research Board.
Olsen, M.J., Hurwitz, D.S., Kashani, A.G., Buker, K., 2015. 3D Virtual Sight Distance Analysis using Lidar Data. Pacific Northwest Transportation Consortium p. 74.
Recarte, M.A., Nunes, L.M., 2000. Effects of verbal and spatial-imagery tasks on eye fixations while driving. J. Exper. Psychol.: Appl. 6 (1), 31.
Sivak, M., 1996. The information that drivers use: is it indeed 90% visual? Perception 25 (9), 1081–1089.
Soilán, M., Riveiro, B., Martínez-Sánchez, J., Arias, P., 2017. Segmentation and classification of road markings using MLS data. ISPRS J. Photogramm. Remote Sens. 123, 94–103.
Tsai, V.J., 1993. Delaunay triangulations in TIN creation: an overview and a linear-time algorithm. Int. J. Geograph. Inform. Sci. 7 (6), 501–524.
Tsai, Y., Yang, Q., Wu, Y., 2011. Use of light detection and ranging data to identify and quantify intersection obstruction and its severity. Transport. Res. Rec.: J. Transport. Res. Board 2241, 99–108.